THE JOURNAL OF PHYSICAL CHEMISTRY C
A JOURNAL OF THE AMERICAN CHEMICAL SOCIETY

pubs.acs.org/JPCC

Article

Stereodynamic Effects of CO Molecules Scattered from a Graphite Surface

Maria Rutigliano* and Fernando Pirani

Cite This: J. Phys. Chem. C 2021, 125, 9074–9084

Read Online

ACCESS | Metrics & More | Article Recommendations | Supporting Information

ABSTRACT: The scattering of CO molecules from a graphite surface has been characterized by exploiting molecular dynamics simulations, based on a chemical state-to-state semiclassical collisional method, and adopting a new reactive potential energy surface that considers the proper treatment of long-range noncovalent interactions promoting the physisorption. Carbon monoxide molecules impinge the surface in well-defined initial rotovibrational states and with the collision energy varying from subthermal up to hyperthermal values. The simulations predict that scattering events occur through both single- and multi-bounces and the initial vibrational state is preserved. In the multibounces instance, molecules tend to be trapped in the physisorption well, especially for collision energies lower than the thermal one. For medium−high collision energies, the scattering occurs mainly via a single-bounce mechanism. The heteronuclear character of the molecule brings out a new intriguing stereodynamic effect, in addition to those highlighted for homonuclear molecules: due to the anisotropic physisorption attraction, the molecule C-end bends toward the surface while approaching this latter. This effect produces evident propensities in the final rotational distributions of the CO scattered molecules.

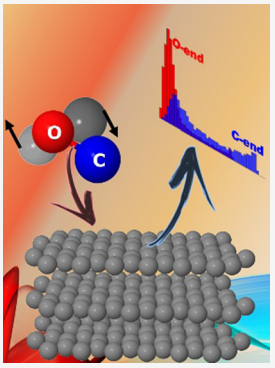

1. INTRODUCTION

Over the last decades, atom/molecule-surface interactions have increasingly attracted interest as they trigger processes concerning many and different applicative and technological fields. This great attentiveness was also accompanied by the contemporary developing and setting-up of increasingly sophisticated and accurate investigation techniques, exploiting both theoretical−computational and experimental methods. In this scenario, graphite and graphite-based materials have drawn great attention, playing a significant role in the chemical physics that controls both formation and interaction of astrobiological molecules (see for instance refs 1, 2), as well as technological processes of interest for ion sources (see for instance refs 3, 4), fusion devices (see for instance refs 5, 6), and sensors (see for instance refs 7, 8). In all of these fields, the energy content of molecules is crucial since it can improve or dampen the efficiency of the elementary step of each reaction and, consequently, of the entire process in its whole.

For this reason, we have undertaken the study of the interaction of light molecules, with well-defined internal energy, with a graphite surface. In the previous investigations[9−11] some selectivity and peculiarities, together with stereodynamic effects, have been pointed out for H_2 (and its isotopologue molecules[12]), O_2, and N_2 molecules using chemical molecular dynamics (MD) simulations in conjunction with an accurate formulation of the interaction potential energy surface (PES), which drives the collision dynamics. In particular, the adopted formulation exploits an improved Lennard-Jones (ILJ) model[13] that represents the long-range interaction, playing a key role in the trapping of gaseous molecules on surfaces, with a high degree of accuracy based on the intrinsic physical properties of interacting species. Proper treatment of long-range interactions appears necessary, as these latter affect all of the basic features of the precursor state that promotes the subsequent evolution of surface processes. Thus, under such conditions, meaningful chemical MD simulations can be performed, by exploiting a state-to-state semiclassical collisional model,[14] to determine the internal energy of the molecule and the energy exchanged with the surface during the trajectory propagation.

In this work, we adopt this well-tested computational setup that has given results consistent with both experimental observations[15,16] and theoretical simulations, conducted with different methodologies for O_2[17,18] and N_2,[19,20] to investigate the interaction of CO molecules with a graphite surface.

Experimental information on the dynamics of collisions between gaseous CO molecules and a graphite surface is somewhat limited. Angular distributions of CO molecules scattered from graphite have been determined in ref 21 for the collision energy from 0.275 eV up to 0.6 eV and for the surface temperature from 150 to 400 K. The experimental results have been analyzed using a molecular scattering model based on

Received: January 21, 2021
Revised: March 29, 2021
Published: April 26, 2021

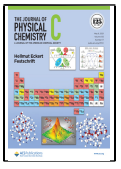

https://doi.org/10.1021/acs.jpcc.1c00555
J. Phys. Chem. C 2021, 125, 9074−9084

classical mechanics, leading to the conclusion that the scattering occurs basically through a single collision, to which a large cooperative motion of carbon surface atoms contributes. Except for the paper of Oh et al.,[21] to the best of our knowledge, there are no other studies in the literature concerning the characterization of CO scattering from graphite probing a wide range of collision energies and different initial rotovibrational states. However, in dated experimental studies, the CO adsorption properties have been investigated. Temperature-programmed results have been reported, in ref 22 for desorption of CO molecules on graphite at room and higher temperatures by underlying the reactive and kinetic properties of CO after adsorption. The sticking probability for CO on graphite resulted very low, as already stated in ref 23.

Furthermore, a detailed picture of elementary processes promoted by collisions and adsorption of CO on metallic and nonmetallic surfaces, of general great relevance both for the control of catalytic reactions and their application for the production of ecofriendly devices and for the industrial Fischer−Tropsch synthesis, can be found in the literature (see for instance refs 24−27).

Therefore, the present study is mostly addressed to define an accurate PES, which controls the interaction of the carbon monoxide molecule with the graphite surface, and to determine the peculiarities of the final results of this interaction, for different and well-defined initial molecular states and different collision energy regimes. The influence of the molecular heteronuclear feature on the reaction dynamics will also be highlighted and discussed.

The present article is organized as follows: In Section 2, the adopted computational setup is described with particular focus on the formulation and features of the PES for the interaction under study. In Section 3, the main obtained results will be presented and discussed in detail. Finally, in Section 4, some conclusions are drawn.

2. COMPUTATIONAL METHODS

The basic features of the scattering of carbon monoxide molecules in well-defined initial rotovibrational states (j_i, v_i) from a graphite surface have been studied by exploiting MD calculations. The used method treats collision events semiclassically[14] and has been successfully applied over the last years to highlight the main selectivity and peculiarities of hydrogen, oxygen, and nitrogen molecules interacting with the same graphite surface.[9−11] In the past, it has been adopted to describe the dynamics of elementary gas-surface processes involving atoms/molecules with different surfaces (see for instance refs 28−30 and references therein). The method, based on the assumption that each collision event can be characterized by solving the relevant three-dimensional (3D) Hamilton's equations of motion self-consistently with the dynamics of the lattice phonons, also includes the evaluation of the molecular state-to-state transitions associated with the internal degree of freedom rearrangement. The complete Hamiltonian for a diatomic molecule interacting with the surface is given by

$$H = \frac{1}{2}\sum_i \frac{P_i^2}{m_i} + V(r_{C-O}) + \Delta E_{ph} + V_{eff}(t,\ T_S),\quad i = 1, 2 \tag{1}$$

where P_i is the momentum of the ith atom having a mass m_i of the impinging molecule, $V(r_{C-O})$ is the intramolecular potential of CO molecules in the gas phase, and ΔE_{ph} is the energy exchanged with the surface phonons. $V_{eff}(t,\ T_S)$ represents the effective potential of the mean field type, depending on the interaction time (t) and the surface temperature (T_S), and obtained as the expectation value of the phonon wave function on the interaction potential, V_{int}, given by the next eq 3:

$$V_{eff}(t,\ T_S) = \langle\psi(t,\ T_S)|V_{int}|\psi(t,\ T_S)\rangle \tag{2}$$

$\Psi(t,\ T_S)$ being the total wave function of the phonon modes given as a distribution of quantum states at a fixed surface temperature T_S. The time evolution of $|\Psi(t,\ T_S)\rangle$ is obtained by solving the time-dependent Schrödinger equations of motion for a set of $(3N - 6)$ independent harmonic oscillators, N being the total number of atoms in the lattice, perturbed by the external forces exerted between the gas-phase species and the surface. V_{int} is expanded up to the linear term in the phonon normal mode coordinates so that the linearly forced harmonic oscillator (LFHO) analytical solution of the quantum equations of motion for the lattice phonons can be assumed. The interested reader can find in refs 14, 28 more details on the evaluation of the terms in eqs 1 and 2.

The adopted method treats the molecular translational motion classically, whereas populated rotational and vibrational degrees of freedom (the latter, represented as Morse oscillators[31]) of scattered molecules are assessed in terms of the action-angle variables using the semiclassical quantization rules.[32] Accordingly, the internal energy of the interacting molecule is partitioned, at each trajectory time step, into vibrational and rotational contributions using equations that include rotational angular momentum and related spectroscopic constants. Thus, this treatment does not enable us to predict some features coming from quantum effects and selection rules.

Before proceeding in the integration of Hamilton's equation, it is necessary to determine both the dynamics of phonons for the considered graphite 3D crystal and an accurate PES driving the reaction under study. Here, we consider the same graphite crystal and, consequently, the same phonon frequency distribution of refs 9−11. Therefore, the graphite 3D crystal lattice used in the calculations consists of 186 carbon atoms, disposed on three layers according to the appropriate lattice symmetry.[33] Instead, the PES is formulated according to the following expression

$$V_{int}(r_{C-O}, R) = \sum_{N}^{k=1}\sum_{2}^{i=1} V_{CO-graphite}(R_{ki})*f_{sw}(r_{C-O}) + \sum_{k=1}^{N}(V_{C-graphite}(R_k) + V_{O-graphite}(R_k))*(1-f_{sw}(r_{C-O})) \tag{3}$$

where $V_{CO-graphite}$, $V_{C-graphite}$, and $V_{O-graphite}$ represent the interaction potential among the CO molecule, C atom, and O atom, respectively, with the adopted surface model, obtained as a sum of pairwise interaction contributions. R is the distance between the kth carbon atom in the lattice and C($i = 1$)/O ($i = 2$) atom in the molecule, for the first term on the right side of eq 3, or the distance between the kth carbon atom in the lattice and the C/O atom, for the second term. $f_{sw}(r_{C-O})$ is a weight

https://doi.org/10.1021/acs.jpcc.1c00555
J. Phys. Chem. C 2021, 125, 9074−9084

function that switches the interaction potential between $V_{CO-graphite}$ and $V_{C/O-graphite}$ as r_{C-O}, the intramolecular distance, increases. The analytical expression of $f_{sw}(r_{C-O})$ is the same used in the building up of reactive PES in the previous study on the interaction of the molecules with graphite.[10,11] This weight function is chosen to provide a quick switching between 1 and 0, preserving the values of $V_{CO-graphite}$ and $V_{C/O-graphite}$ for r_{C-O} lower and higher, respectively, of the intramolecular distance considered critical for CO molecule dissociation (r_{diss} = 3.5 Å).[34] The potential is obtained as a sum of both components, weighted according to the f_{sw} (r_{C-O}) value, in the range of distances at which the switch occurs. For its intrinsic formulation, the adopted PES is reactive, in the sense that it allows us to consider all possible reaction channels, including dissociation that can occur when the CO molecule interacts with the surface.

The interaction of carbon monoxide molecules with graphite/graphite-based surfaces gives rise to a physisorption state whose binding energies have been determined using different models and methods at different degrees of accuracy. In ref 1, the interaction potential experienced by CO molecules, adsorbed on the graphite basal plane has been estimated using a Lennard-Jones (LJ) potential modified to account for the anisotropic polarizability of the C atom in the substrate to which have been added electrostatic and induction contributions. From the resulting PES, it appears that the CO molecule takes an equilibrium configuration when is in a nearly flat orientation position with respect to the surface plane. This configuration corresponds to a distance of 3.08 Å above the center of the graphite hexagonal unit cell and a minimum energy value of −0.12 eV. Another relative energy minimum (−0.107 eV) is found when the molecule is at a distance of 3.24 Å on the carbon atom. Moreover, the PES exhibits a saddle point in the diffusion path of the molecule on the surface, when its center of mass (CM) is on the bridge site. However, it should be noted that in ref 1, the Lorentz and Berthelot combination rules have been used to determine the LJ pair interaction parameters, and it is widely recognized that these rules should be used with great caution as they give reliable results only for very similar pairs of partners interacting through pure van der Waals forces.

Values of the interaction energy in the range [−0.11; −0.15] eV and for equilibrium distances around 3.2 Å for CO interacting with coronene or graphene are reported by Rubeš et al.[35] for the minimum configuration, in which the molecule is parallel to the surface with the O atom on the center of the six-membered ring. Therefore, a density-functional theory/coupled cluster method has been adopted to describe weakly bound molecular systems and to reduce the physisorption energy overestimation provided by DFT calculations at the MP2 level.

The adsorption energy and the corresponding distance between CO and the graphene sheet have also been calculated to be around −0.12 eV and 3 Å in ref 36 using DFT calculations with the plane-wave basis set and periodic boundary conditions. On the contrary, Möller−Plesset ab initio quantum chemistry methods have been used in ref 37 to consider the effect of London dispersion energy that plays a role in the interaction of molecules with surfaces. The obtained minimum interaction energy value was nearly −0.080 eV, corresponding to an equilibrium distance of 3.5 Å. All of these results highlight the difference in the data available in the literature for the CO−graphite interaction potential. Alongside these values determined by various theoretical−computational approaches, the binding energy value of 0.11 eV for the CO−graphite interaction reported by Vidali et al.[38] and determined by a thermodynamic experiment[39] should also be mentioned.[39]

Most of the elementary surface processes, promoted by CO−graphite collisions, are driven surely by the noncovalent intermolecular interactions, dominant at intermediate and large separation distances between the gas-phase species and surface and that control the physical adsorption. However, for a proper assessment of the collision dynamics, it is fundamental to describe the interaction in the full space of permitted orientations of the reagent molecule with respect to the surface. Accordingly, in this investigation $V_{CO-graphite}$ is obtained as a sum of (effective atom)−(effective atom) pair interaction contributions, each one represented by an improved Lennard-Jones (ILJ) formulation,[13] depending on the pair distance R and having the following analytical expression

$$V_{ILJ}(R) = \varepsilon\left[\frac{m}{n(R)-m}\left(\frac{R_m}{R}\right)^{n(R)} - \frac{n(R)}{n(R)-m}\left(\frac{R_m}{R}\right)^{m}\right] \quad (4)$$

with

$$n(R) = \beta + 4\left(\frac{R}{R_m}\right)^2 \quad (5)$$

The first term of eq 4 describes the size repulsion, while the second one the attraction. The parameters ε and R_m, which represent the potential well depth and its location, respectively, for the considered pair, define the strength of both terms in eq 4. β is an additional parameter depending on the "hardness" of the two partners. For the neutral−neutral interactions, as the present ones, m = 6 must be used: in these cases, the ILJ function provides for each interacting pair an asymptotic dispersion attraction associated with a C_6 coefficient defined as $C_6 = \varepsilon R_m^6$.

It should be noted that the ILJ potential function removes most of the inadequacies of the well-known, and widely used, LJ model due to an excessive repulsion at short range and a too strong attraction at long range. Therefore, the adopted potential formulation appears suitable to fulfill the request concerning the right description of noncovalent long-range interactions in the full space of the relative configurations of the interacting systems, above stressed. Since at large separation distances the partners maintain most of their individual properties, parallel efforts have been addressed to the search of correlations among the strength, range, and anisotropy of the interactions with basic physical properties of involved partners, as the electronic polarizability[40] (see also ref 41 and references therein).

Zero-order values of the parameters defining the CO−graphite interaction have been estimated (see refs 13, 40 and references therein) by exploiting the polarizability of the single C/O atom (1.76/0.80 Å^3) and the effective polarizability values of C (in CO) and O (in CO) (1.3 and 0.65 Å^3, respectively) and of the C atom in graphite (1.3 Å^3), which are the fundamental physical properties controlling both the size repulsion and the dispersion attraction. Such values have also been fine-tuned, within limited ranges, to provide results internally consistent with those previously obtained for O_2-/N_2- graphite systems,[10,11] as the correct description of the

https://doi.org/10.1021/acs.jpcc.1c00555
J. Phys. Chem. C 2021, 125, 9074−9084

long-range C_3 dispersion coefficient sequence. This latter coefficient describes the asymptotic global dispersion attraction of a gaseous species with all atoms of the surface having a density ρ (0.1133 atoms/Å^3 for graphite) and is given by the well-known relation between C_6 and C_3:[42] $C_3 = (\pi C_6 \rho)/6$.

In Table 1 the values, so obtained, of parameters used in this work are reported together with the C_6 and C_3 dispersion coefficients. The results in Table 1 suggest that a total C_3 coefficient, equal to 1377.91 meV Å^3, can be associated with the CO−graphite interaction. Unfortunately, in the literature, to our knowledge, a value for this coefficient is not available.

Table 1. ILJ Parameters Used in the Calculations and Derived Dispersion Coefficients

	ε (meV)	R_m (Å)	β	C_6 (meV Å^6)	C_3 (meV Å^3)
C(CO)−C interaction	4.74	3.8	8.0	14271.84	846.66
O(CO)−C interaction	3.85	3.64	8.0	8955.07	531.25
C−C interaction	5.83	3.8	8.0	17553.76	1041.35
O−C interaction	4.62	3.62	8.0	10396.65	616.77

However, some considerations based on the available data lead us to be confident of the result determined here. Indeed, we would expect for C_3 a value intermediate between those known for the O_2 molecule (polarizability equal to 1.6 Å^3) and the Kr atom (polarizability equal to 2.49 Å^3), considering that the CO molecular polarizability is equal to 1.96 Å^3. Furthermore, it should also be considered that the CO molecule has a small electric dipole moment and then, even if minimally, an inductive term could also add to the C_3 coefficient obtainable by considering only the dispersion.

The C_3 values for the O_2−graphite and Kr−graphite interaction, as reported by Vidali et al.,[38] are 1157 and 1760 meV Å^3, respectively. Therefore, the C_3 coefficient here determined for the CO−graphite interaction places well in the range just predicted. Moreover, the C_3 value determined here is also greater than that obtained for the O_2−graphite interaction[10] using the same interaction description.

The ILJ interaction potential, as obtained using the parameters of Table 1, for the CO molecule interacting with the molecular axis parallel and perpendicular on the three high symmetry sites of graphite, namely, on top of a C atom (T), on the bridge (B) site, and above the center of the hexagonal cell (HC), is reported in Figure 1a−d as a function of the Cartesian coordinate of the molecular center of mass (CM) normal to the surface plane in the assumed reference frame (Z_{CM}).

It appears that the ILJ potential for CO impinging in the parallel configuration (Figure 1a) is almost independent (with differences of the order of some meV) of the surface site and has a minimum physisorption energy of ∼−0.125 eV

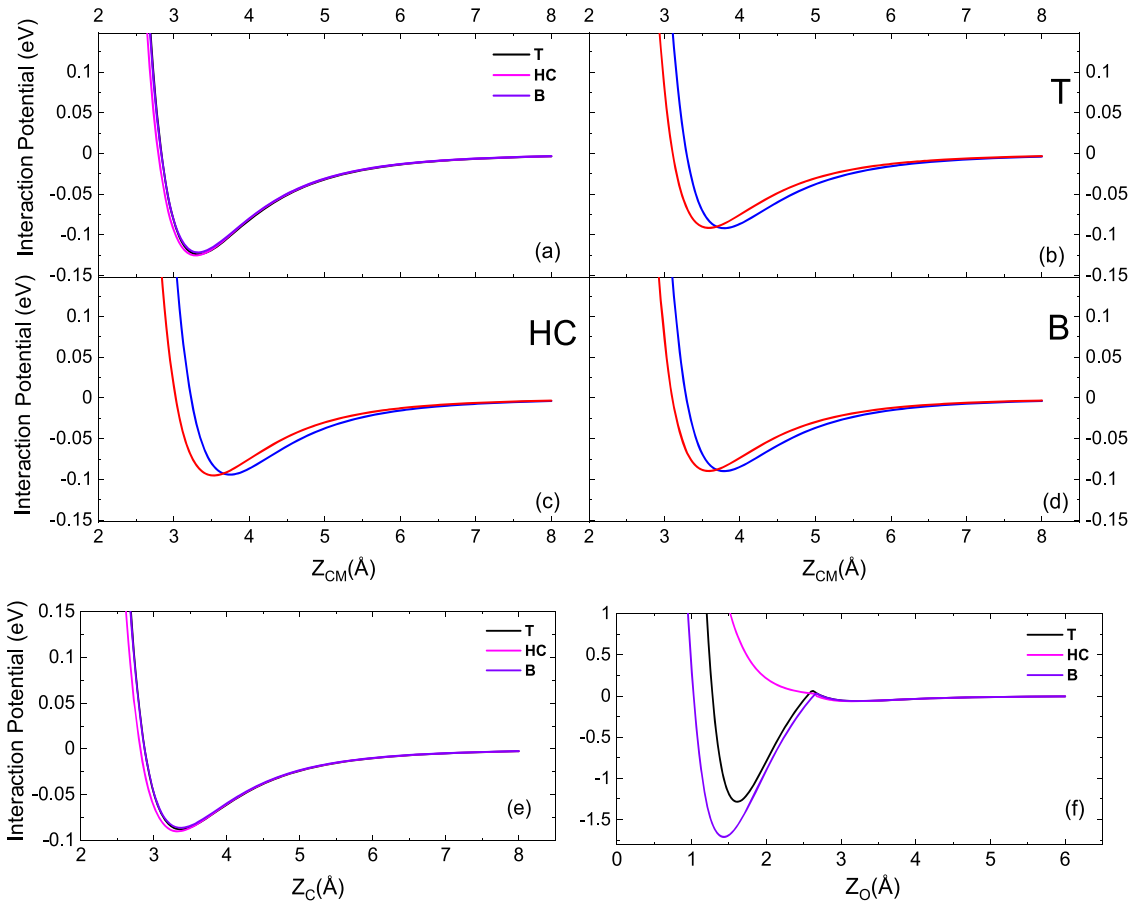

Figure 1. ILJ potential for the CO molecule interacting on the three high symmetry sites of graphite in (a) parallel and (b)−(d) perpendicular configurations. In panel (b)−(d) CO molecule impinges with the C-end (blue line) or O-end (red line) facing toward the surface. (e) ILJ for the C atom interacting with the graphite surface. (f) Interaction potential determined in ref 10 for the O atom interacting with graphite, including short- and long-range (ILJ) interactions.

https://doi.org/10.1021/acs.jpcc.1c00555
J. Phys. Chem. C 2021, 125, 9074−9084

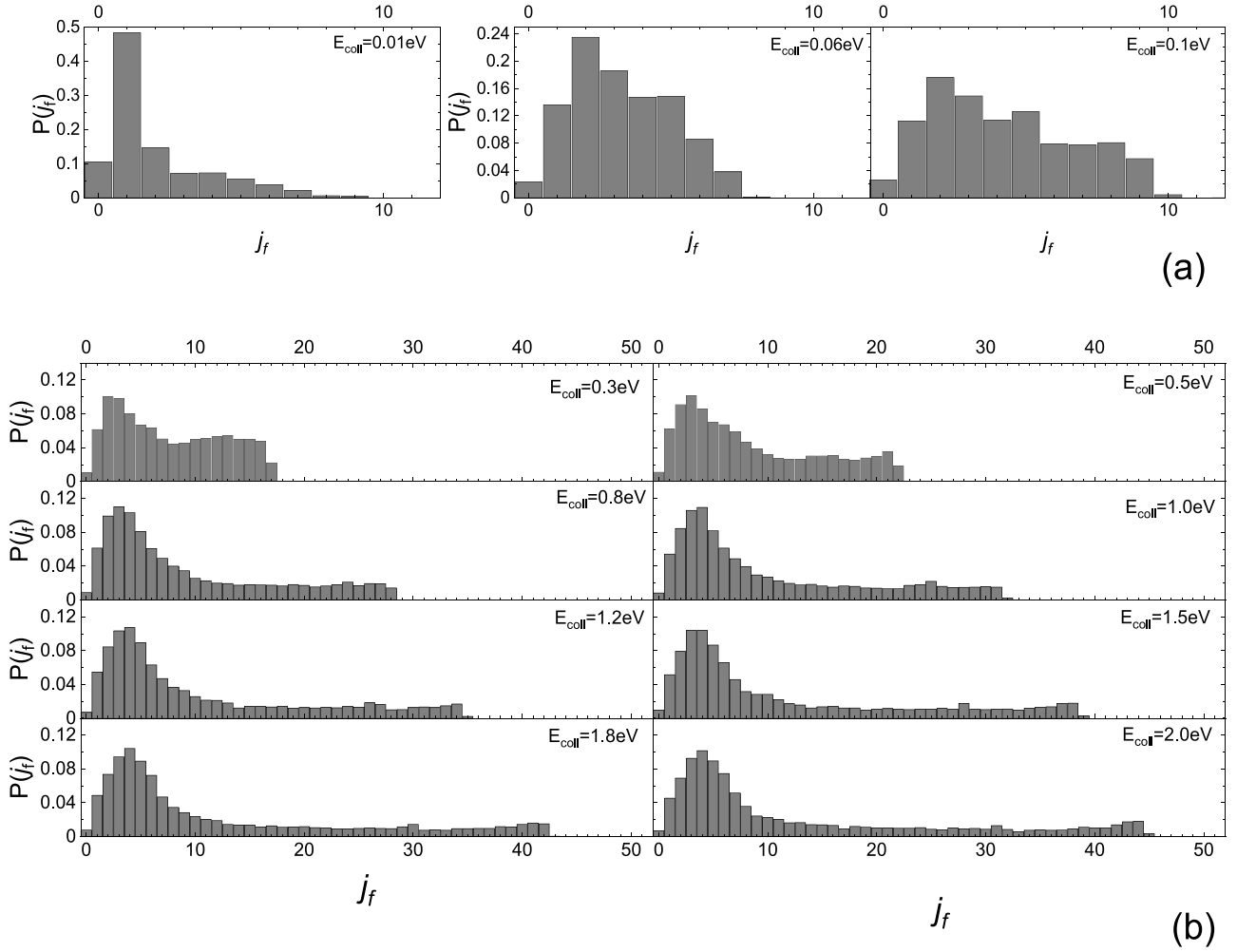

Figure 2. (a) Final rotational distribution for CO (0, 0) molecules scattered by the graphite surface for the three lowest E_{coll} values and (b) same as (a) but for higher collision energies.

corresponding to a bond length of 3.325 Å. The main difference occurs when the molecule impinges with the molecular axis along the normal to the surface. In fact, in this case, although the physisorption energy roughly assumes the same values (see Figure 1b–d), a shift of the minimum distance occurs according to the molecule approach with the C-end or O-end toward the surface. Approximately, the minimum energy is −0.09 eV for Z_{CM} of 3.7/3.8 or 3.5/3.6 Å, depending on whether the molecule impinges with the C-end or O-end facing the surface. The obtained values for the minimum energy and bond length compare well with the results obtained at the DFT level for the corresponding configuration reported above.

Therefore, this finding and the partial contribution of the two atoms (which differ by almost 50%) to the global C_3 (see Table 1) would indicate that the molecule C-end is more strongly attracted than the O-end by the surface. This occurrence suggests the possibility that the molecule, impinging in very low-lying initial rotational states (j_i), even in the parallel configuration, could tend to bend to have the C-end toward the surface. But this effect can affect the trajectories even at higher collision energies, also depending on the impact site. To obtain a reactive PES, it is also necessary to include the potentials for the C/O atom interacting with the surface; to this end, we consider the second term on the right side of eq 3.

$V_{C-graphite}$, expected to be of pure noncovalent nature, has been fully represented by the ILJ potential and it is plotted in Figure 1e, from which we can deduce that its values do not differ for the C incident on T and B sites, while a small deviation in the repulsive part and a bit greater physisorption energy is obtained when the C atom impinges on the HC site.

Instead, $V_{O-graphite}$ is the same potential determined by us in ref 10 for the interaction of the O atom with the graphite surface, including both short-[43] and long-range ILJ interactions, and it is reported in Figure 1f.

The simulations involve integrating the complete Hamiltonian of eq 1 describing the interaction for fixed initial conditions. We propagate and examine 15 000 trajectories for each considered set of initial rotovibrational states and collision energy, assuming a fixed value for polar and azimuthal angles of the impinging CM molecule ($\theta = \phi = 0°$ define the selected normal approach), while the azimuthal angle of the molecular axis is randomly determined for each trajectory. The surface temperature is fixed to T_S = 100 K. The initial coordinates of both atoms in the molecule are chosen randomly in an aiming area on the surface, large enough and at the same time such as to prevent the edge effects during the trajectory propagation. The integration step is 0.25 fs and the accuracy required in the integration procedure is 10^{-8}.

https://doi.org/10.1021/acs.jpcc.1c00555
J. Phys. Chem. C 2021, 125, 9074−9084

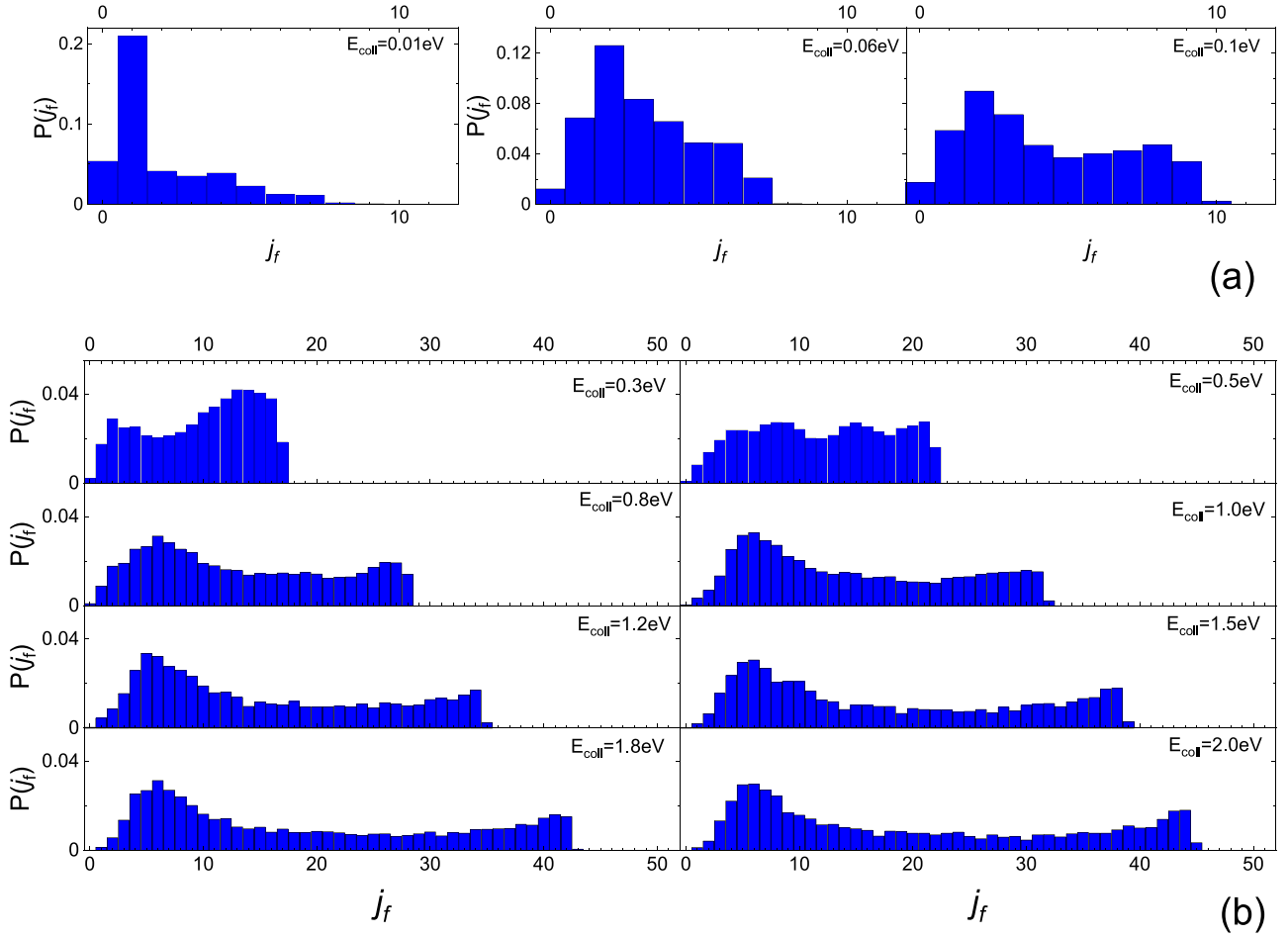

Figure 3. Same as Figure 2 but for CO molecules impinging with the C-end toward the surface.

In the simulations, in addition to the ground state, we have considered the medium excited vibrational state $v_i = 5$ and excited low−medium rotational levels $2 \leq j_i \leq 5$ and $j_i = 10$, 15. The CM collision energy (E_{coll}) has been spanned on a wide range of values, going from 0.01 eV (subthermal conditions) up to 2.0 eV (hyperthermal conditions).

The adopted reactive PES enables us to describe and follow the different elementary surface processes occurring when the CO molecule impinges on the surface: molecular scattering, molecular adsorption, dissociative adsorption with adsorption of both atoms, dissociative adsorption that can be followed by the desorption of one atom, while the other remains trapped on the surface, or by the desorption of both atoms.

The criteria adopted in the present analysis, leading to the assignment of a given trajectory to one of the previously listed reaction channels, are similar to those used in refs 9−11. So, molecular scattering occurs if, after the interaction with the graphite surface, the intramolecular distance (r_{C-O}) is lower than r_{diss} and at the same time the distance between its CM and the surface is larger than 8.0 Å. On the contrary, if, after the interaction with the graphite surface, the distance between its CM and the surface is smaller than 5.0 Å and $r_{C-O} < r_{diss}$ the molecule is considered trapped in the physisorption well, while if $r_{C-O} > r_{diss}$ the molecule is dissociated and the possible fate of the trajectory is one of those mentioned above.

The maximum propagation time for the trajectories is very long and fixed at 30 000 fs; the trajectory is discarded and not considered in determining probabilities if none of the previous criteria are satisfied, elapsed this time.

As said previously, the method does not consider any selection rule, and then the rotovibrational states are determined as continuous variables.

3. RESULTS AND DISCUSSION

The behavior of the CO molecule, in different and well-defined initial rotovibrational states (j_i, v_i), impinging along the normal direction on the graphite surface, has been investigated deeply. The results reported in the following have been identified as the most proper to emphasize basic selectivity and propensities in the scattering mechanism. In the Supporting Information (SI), additional details on the final distributions, corresponding to the complete set of initial states considered in this study, can be found. The results of simulations performed at $v_i = 0$ and 5 predict that the initial vibrational state, as already observed for O_2 and N_2 molecules interacting with the same graphite surface, is also preserved for the CO molecule.

For the conditions simulated here, the analysis of the trajectories reveals that the only two occurring processes are molecular adsorption and molecular scattering. Molecular adsorption is predicted only for $v_i = 0$ and $E_{coll} \leq 0.1$ eV, with decreasing probabilities as both E_{coll} and j_i increases: the maximum value (0.77) occurring for $j_i = 0$ and $E_{coll} = 0.01$ eV. Instead, its probability is zero for $v_i = 5$, even at the lowest collisional energies. At the lowest E_{coll} value, a significant percentage of trajectories is practically not classifiable, despite

https://doi.org/10.1021/acs.jpcc.1c00555
J. Phys. Chem. C 2021, 125, 9074−9084

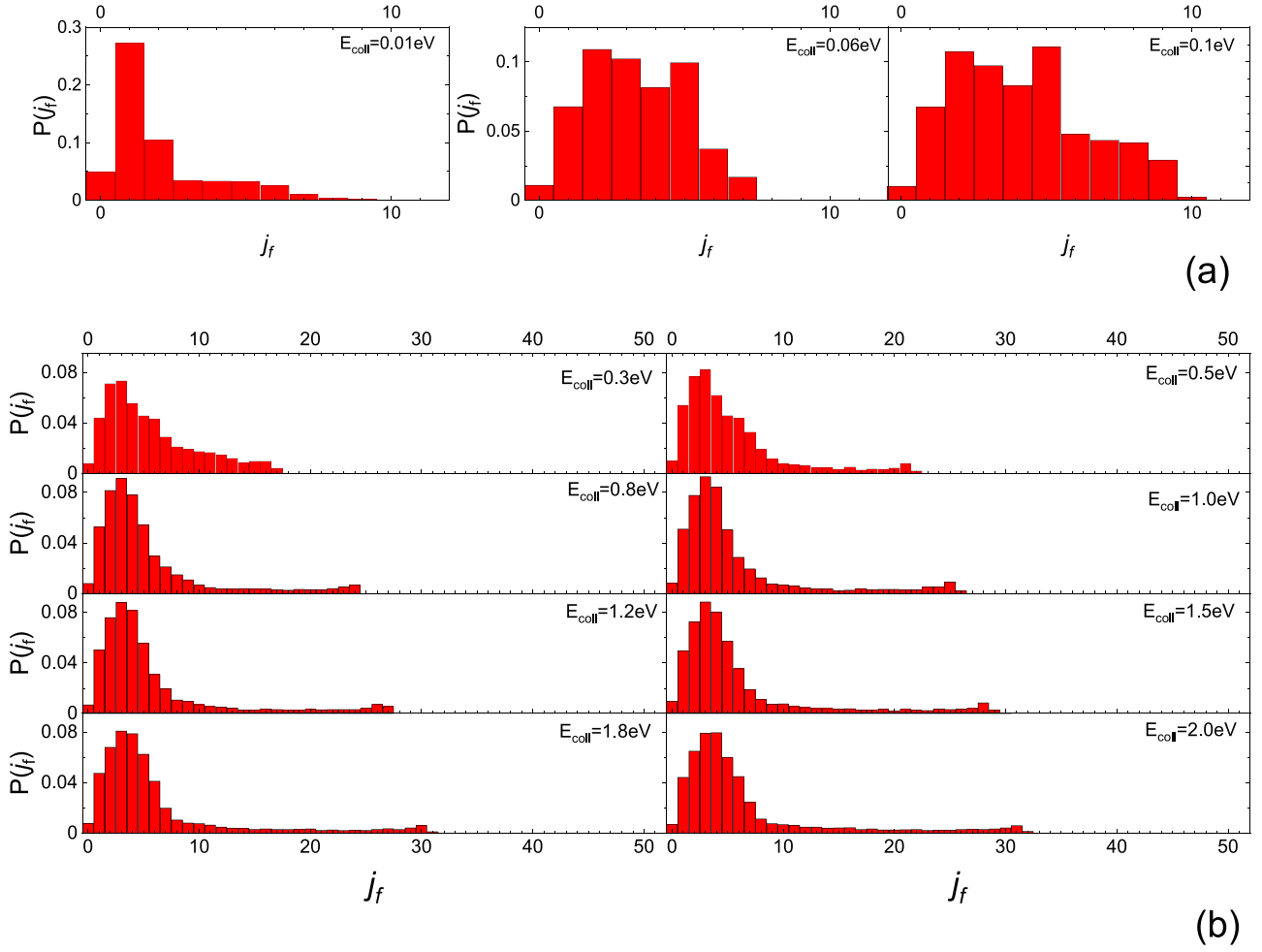

Figure 4. Same as Figure 2 but for CO molecules impinging with the O-end toward the surface.

the allowed long propagation times (up to 30 000 fs), as found in refs 10, 11. This is because the CO molecules remain in a sort of "metastable" state, characterized by continuous bounces on the surface due to the physisorption phenomenon, controlled by the noncovalent interaction potential well, located at an intermediate separation distance from the surface. As a consequence, the interaction dynamics appears to be mainly determined by the initial rotational state. Then, in the following, the focus is on the analysis of the obtained results for $v_i = 0$, referring the interested reader to the SI where the complete set of obtained results, including those for $v_i = 5$, is reported. In this perspective, in Figure 2 the distributions of final rotational levels (j_f), obtained for CO molecules in the ground rotovibrational state scattered from the graphite surface, are shown. Moreover, while the complete set of final rotational distributions for j_i values higher than the lowest one is reported in the SI, their relevant details are discussed below in connection with those obtained for the ground state.

A careful examination of Figure 2 reveals that final rotational distributions exhibit different features for E_{coll} lower and higher than 0.3 eV, respectively. In particular, as E_{coll} increases starting from such a reference value, the distributions are characterized by the gradual appearance of both the well-defined main peak located approximately between $j_f = 3$ and 5 and the tail extending to higher j_f values, where a relative secondary maximum tends to emerge. For collisions under thermal and hyperthermal conditions ($E_{coll} \geq 0.1$ eV), the appearance of secondary maxima in the region of high j_f has already been observed for O_2[10] and N_2[11] molecules and, there, related to phenomena controlled by the rotational alignment and rotational rainbow. On the other hand, for $E_{coll} = 0.01$ eV (subthermal conditions), the distribution exhibits a peak on $j_f = j_i + 1$ for $j_i = 0$, conversely for $0 < j_i \leq 5$, the peak is always placed on $j_f = j_i$. For the two highest j_i values considered in this study (see the SI), CO molecules are most probably scattered and deactivated in the rotational level immediately below j_i. On the contrary, for $E_{coll} = 0.1$ eV and $j_i = 0$, the distribution has a peak in $j_f = j_i + 2$ while as j_i increases (up to 5) the distribution begins to widen and to exhibit a peak around $j_f = j_i + 1$.

To check that the transition in the features of the distributions occurs linearly as the collision energy increases, we considered, for low-lying levels, $j_i = 0$, 1, 2, for which differences in the inelasticity can be better highlighted, an intermediate energy value of 0.06 eV. Obtained results confirm the linear transition when increasing the E_{coll} value. Indeed, while for the lowest E_{coll} value and $j_i = 0$ the peak of the final state distribution (see Figure 2a) is on $j_f = j_i + 1$, already at $E_{coll} = 0.06$ eV the distribution maximum occurs at $j_f = j_i + 2$. As j_i increases, the distribution peak tends to be shifted at $j_f = j_i + 1$ (see the SI).

Since CO is a heteronuclear molecule, it is worth investigating whether there is a link between the end atom of the incident molecule facing/closest to the surface at the beginning of the trajectory and the final rotational state in

https://doi.org/10.1021/acs.jpcc.1c00555
J. Phys. Chem. C 2021, 125, 9074−9084

which it is scattered. Then, we distinguish molecules impinging with the C-end or with the O-end facing toward the surface and redetermine the final rotational distributions. In this way, we obtain the results shown in Figures 3 and 4 for CO (0.0).

By comparing the distributions of Figures 2−4, we can affirm that molecules impinging with the O-end facing toward the surface give rise to the bell-shaped distribution in correspondence with the low−medium j_f region, instead molecules impinging with the C-end are mainly responsible for the long tails extending to the medium−high j_f region and for the relative secondary maximum. An opposite behavior is observed in the distributions for the two highest values of j_i, in the sense that, under these circumstances, molecules with the C-end toward the surface mainly contribute to the main peak, while those with the O-end affect the distribution tail (see the SI).

The features of the final rotation distributions obtained in the case of $v_i = 5$ do not differ much from those just discussed above for $v_i = 0$, as can be seen in Table 2 where we reported

Table 2. Average Weighted Rotational Number for $v_i = 0$ and $v_i = 5$ (italics)

$j_i \rightarrow$	0	1	2	3	4	5	10	15
E_{coll} (eV)				<j_f>				
0.01	2	2	2	3	3	4	8	12
	2	*2*	*2*	*3*	*3*	*4*	*7*	*12*
0.1	4	4	5	5	6	6	10	14
	4	*4*	*5*	*5*	*6*	*7*	*10*	*14*
0.3	8	8	8	8	9	9	12	16
	7	*8*	*7*	*8*	*8*	*9*	*12*	*16*
0.5	9	9	9	9	9	10	13	17
	9	*9*	*9*	*9*	*9*	*10*	*13*	*17*
0.8	9	9	9	10	10	11	14	18
	9	*9*	*9*	*10*	*10*	*10*	*14*	*18*
1.0	10	10	10	11	11	11	15	19
	10	*10*	*10*	*11*	*11*	*11*	*14*	*19*
1.2	11	11	11	11	12	12	15	19
	10	*10*	*10*	*11*	*11*	*12*	*15*	*19*
1.5	12	12	12	12	13	13	16	20
	11	*11*	*11*	*12*	*12*	*13*	*16*	*20*
1.8	12	13	13	13	13	14	17	20
	12	*12*	*13*	*12*	*13*	*13*	*16*	*20*
2.0	13	13	13	14	14	14	17	21
	13	*13*	*13*	*13*	*14*	*14*	*17*	*21*

the weighted average rotational level (<j_f>) on the complete set of scattered molecules, without distinguishing them according to the end facing the surface, for the two considered v_i values. It appears, from the data in Table 2 that the rotational energy content of scattered molecules depends on j_i and increases as E_{coll} increases. The observed small differences (of the order of 1 unit) can mainly be ascribed to the method used in the determination of the rotational level alongside the trajectory integration.

The microscopic mechanism underlying the interactions has been investigated by performing a careful analysis of the trajectories to better understand the peculiarities highlighted for the scattered molecules, as already done in refs 9−11. First of all, we found that the interaction of the CO molecule with graphite occurs via both single and multibounce mechanisms, with the former less efficient at low E_{coll} and having increasing probabilities of occurring as the collision energy increases. Again, this feature is independent of the initial vibrational number.

In particular, in Figure 5 the probabilities for single and multibounce mechanisms for different end atoms facing the

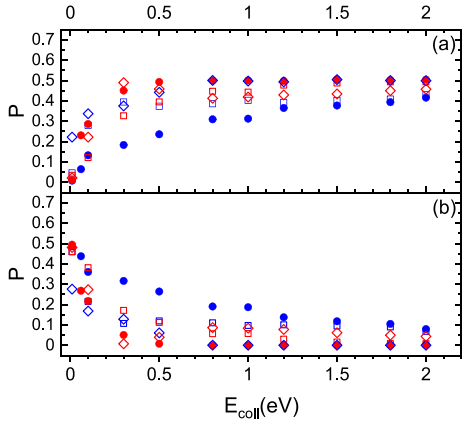

Figure 5. Probabilities for (a) single- and (b) multibounce mechanisms for CO molecules impinging with the C-end (blue symbols) and O-end (red symbols) facing toward the surface for $j_i = 0$ (full dots), 3 (open squares), and 10 (open diamonds).

surface and for the three different j_i values are reported. It appears that with j_i increasing, the probability value for the single-bounce grows and the increase is greater for $E_{coll} \leq 0.1$ eV mainly for C-end molecules. An opposite and complementary behavior is observed for the multibounce probability. This result is contrary to the single collision mechanism predicted in ref 21 where the experimental findings have been interpreted through the classical rigid molecular scattering theory. Therefore, from the results of the present analysis, emerges the importance of using a collision model enabling us to consider in the simulations the individual motion of the two atoms of the molecule during the interaction with the surface, in conjunction with a reactive PES.

Furthermore, from the analysis of the trajectories, it emerges that inelasticity manifests more efficiently when the molecule approaches with the C-end facing the surface. This occurs since the C atom is farther from the molecule's CM and then the resulting lever effect and consequently the acting torque are stronger, providing a more efficient rotational excitation. Moreover, as already underlined in the previous section, the C-end molecule is more efficiently attracted by the surface and at longer distances with respect to the O-end, and this selectivity of the interaction generates a natural molecular bending toward the surface. The influence of the molecule atom-end facing the surface, induced by the potential anisotropy, on the reaction dynamics of the CO molecule was already highlighted in ref 27, although in that case it is due to stronger chemical interactions.

Furthermore, as found in the case of O_2[10] and N_2,[11] CO molecules too impinging with a cartwheel-like motion are scattered in high j_f and mainly through a single bounce independently from the atom facing the surface. Instead, the CO molecule approaching the surface with a helicopter-like motion undergoes distortion and, at the time in which the C-end is facing the surface, realigns beginning to move with a cartwheel-like motion with which it gets away.

This sequence can be observed by carefully looking at Figure 6 where the time evolution along a typical trajectory of the Z

https://doi.org/10.1021/acs.jpcc.1c00555
J. Phys. Chem. C 2021, 125, 9074−9084

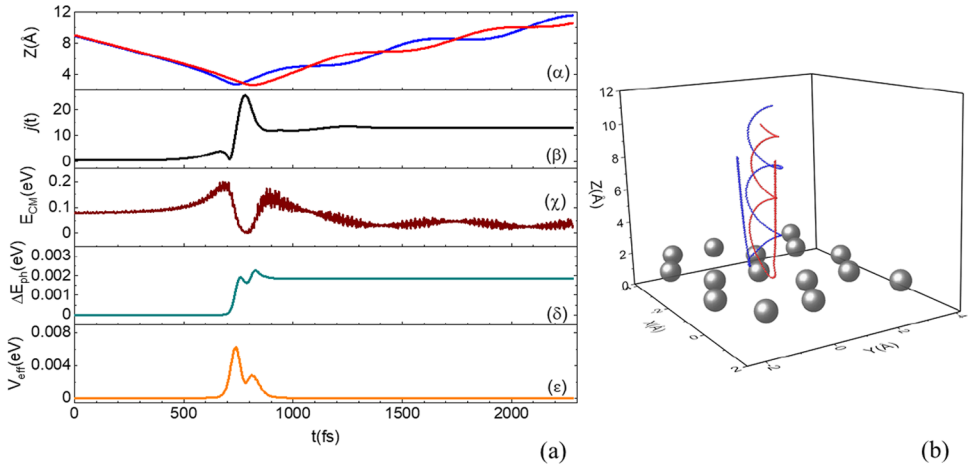

Figure 6. Trajectory for CO (0, 0) at E_{coll} = 0.3 eV backscattered in the gas phase in CO (0, 13). (a) Panel (α): dependence on the time t of the Z coordinate, for the two atoms in the CO molecule (C atom blue line and O atom red line); (a) panel (β): rotational state evolution along the trajectory; (a) panel (χ): CM translational energy; (a) panel (δ): energy exchanged with the surface phonons along the trajectory; and (a) panel (ε): $V_{eff}(t)$ potential. (b) 3D trajectory (C atom blue line and O atom red line). The C atoms on the first layer of the surface (an up-shift has been made from their position Z = 0) are also reported (dark gray spheres).

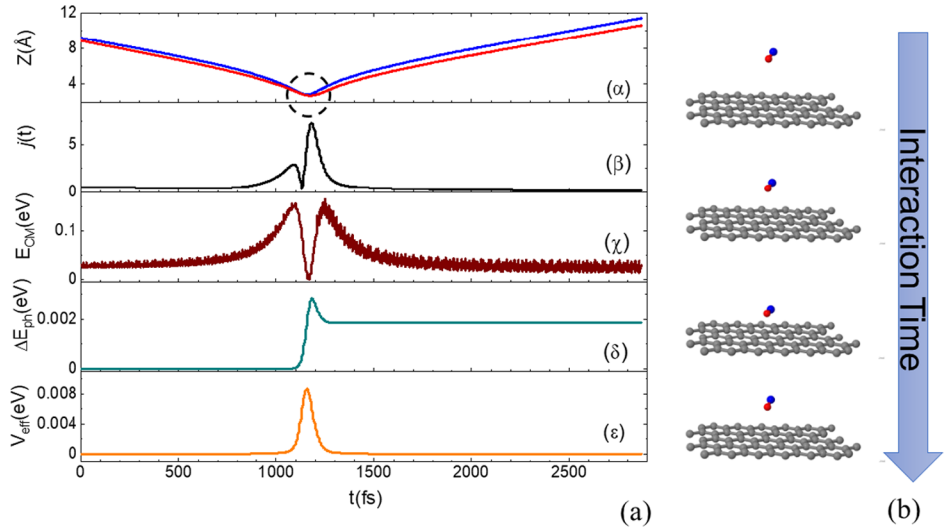

Figure 7. (a) Same as Figure 6 but for E_{coll} = 0.1 eV. The final internal state of the molecule is (0, 0). (b) Snapshots of the trajectory for interaction times in the dashed circle on panel (a).

coordinate (the distance along the normal direction) of both atoms in the molecule, together with the CM translational kinetic energy (E_{CM}), is displayed. The time dependence of the rotational level j of the energy exchanged with the surface (ΔE_{ph}) and of the V_{eff} potential (see eq 1) is also reported.

The main findings, obtained by the analysis of trajectories, can be summarized in the following four points: (1) For the CO molecule, due to the bending effect of the C-end, the outgoing molecules almost always tend to rotate taking a cartwheel-like motion, mainly if the collision is inelastic, with the formation of medium−high j_f. (2) Single-bounce trajectories are observed only for molecules that at the impact time have both C and O atoms parallel or almost parallel to the surface and for nearly elastic collisions (see Figure 7). (3) Single rebound inelastic scattering can occur both if the molecule impacts with the C-end and O-end. In any case, even in this last circumstance, the molecule folds and reorientates so that the C-end should be closer to the surface promoting the molecular diffusion in the gas phase. This behavior is observed mainly for j_i = 0 and E_{coll} = 0.1 eV. (4) Multibouncing scattering occurs with a greater propensity when the C-end faces and is closer to the surface.

In particular, the case of E_{coll} = 0.1 eV is illustrated in Figure 7, where it is observable that a molecule starting at large Z with the O-end faced toward the surface, during the approach tends to be reoriented by the selective stronger attraction undergone by the C-end atom. This selectivity becomes more effective in the vicinity of the closest approach and manifests in reducing the separation distance of the carbon atom from the surface. However, during the motion inversion, the associated stronger repulsion undergone by the C atom determines a faster increase of its separation distance while the molecule escapes from the surface, as displayed in Figure 7b in which snapshots of the molecular configuration with respect to the first layer of graphite are displayed for the interaction times highlighted by the dashed circle in Figure 7a.

By examining Figures 6 and 7, it emerges that for CO scattering from graphite also, the interaction is dominated

https://doi.org/10.1021/acs.jpcc.1c00555
J. Phys. Chem. C 2021, 125, 9074−9084

mainly by the coupling between the rotational (R) and translational (T) molecular internal motions. Indeed, a high increment of the rotational excitation can occur when the molecule approaching the surface is slowed. However, when it is backscattered in the gas phase, the energy stored in the rotational degree is given back mainly to the translational motion while the energy exchanged with the surface phonons is small according to the weak physisorption interaction underlying the process.

Finally, in Figure 8, the angular distributions of reflected molecules are displayed. By looking at Figure 8, it emerges that

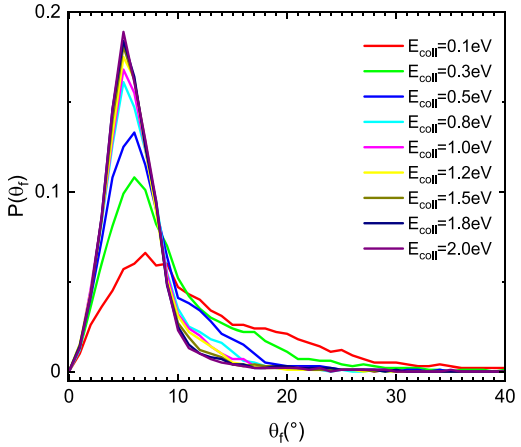

Figure 8. Angular distributions of backscattered CO molecules impinging in the rotovibrational ground state.

the latter become narrower, as the collision energy increases, around the peak placed in $\theta_f \sim 6°$, in agreement with what is measured in ref 21, predicting angular distributions with a peak in a slightly supraspecular direction. However, our distributions show non-negligible values for final angles in the range $10 < \theta_f < 20°$, mainly for the three lowest collision energies. The deep investigation of the trajectories giving these larger values of θ_f leads to assessing that most of these collision events occur when the molecule O-end is facing the surface, undergoing stronger interactions at shorter distances. Therefore, this finding is still strictly related to the PES anisotropy.

4. CONCLUSIONS

The role of stereodynamic effects on the CO molecule scattering from a graphite surface has been highlighted using a new and accurate reactive PES, including proper analytical treatment of long-range interactions in the full space of the relative configurations, in conjunction with chemical state-to-state molecular dynamics simulations.

As already stated for the scattering of O_2[10] and N_2[11] from the graphite, CO molecules are also scattered from the surface in excited rotational states if they impinge with an internal cartwheel-like motion, while they preserve or slightly change the initial rotational state if they collide with an internal helicopter-like motion. In addition to these peculiarities, the heteronuclear nature of the carbon monoxide molecule and the resulting different attraction/repulsion of the C-end compared to the O-end give rise to new stereodynamic effects, observable especially at a low collision energy, when the collision times become sufficiently long allowing for molecular reorientation effects.

In particular, significant differences between the chemical (O-end) and noncovalent (C-end) interactions have been emphasized, highlighting the C-end bending toward the surface as the molecule approaches this latter. These differences also appear in the final rotational distributions in which peaks in the low j_f values are mainly due to the molecules impinging with the O-end closer to the surface, while tails for higher j_f values are primarily attributable to molecules approaching with the C-end toward the surface. This behavior is also tightly related to the observation that inelastic scattering, through both single-/multirebound mechanisms, occurs with evident propensity when the C-end is closer and facing the surface. Such behavior for CO interactions with a metallic surface[25,26] has not been observed.

■ ASSOCIATED CONTENT

Supporting Information

The Supporting Information is available free of charge at https://pubs.acs.org/doi/10.1021/acs.jpcc.1c00555.

Final rotational distributions of CO molecules backscattered in the gas phase as a function of the impinging energy and for different initial rotovibrational states (j_i = 0, 1, 2, 3, 4, 5, 10, and 15; v_i = 0, 5) (PDF)

■ AUTHOR INFORMATION

Corresponding Author

Maria Rutigliano − *CNR-ISTP (Istituto per la Scienza e Tecnologia dei Plasmi), 70126 Bari, Italy;* orcid.org/0000-0002-2152-0369; Phone: +39 080 5929512; Email: maria.rutigliano@cnr.it

Author

Fernando Pirani − *Dipartimento di Chimica, Biologia e Biotecnologie, Università di Perugia, 06123 Perugia, Italy; CNR-SCITEC (Istituto di Scienze e Tecnologie Chimiche "Giulio Natta"), 06123 Perugia, Italy;* orcid.org/0000-0003-3110-6521

Complete contact information is available at: https://pubs.acs.org/10.1021/acs.jpcc.1c00555

Notes

The authors declare no competing financial interest.

■ REFERENCES

(1) Lakhlifi, A.; Killingbeck, J. P. Investigation of the interaction of some astrobiological molecules with the surface of a graphite (0001) substrate. Application to the CO, HCN, H_2O and H_2CO molecules. *Surf. Sci.* **2010**, *604*, 38−46.

(2) Ehrenfreund, P.; Cami, J. Cosmic Carbon Chemistry: From the Interstellar Medium to the Early Earth. *Cold Spring Harbor Perspect. Biol.* **2010**, *2*, No. a002097.

(3) Tsumori, K.; Koppers, W. R.; Heeren, R. M. A.; Kadodwala, M. F.; Beijersbergen, J. H. M.; Kleyn, A. W. Large ion yields in hydrogen scattering from a graphite surface. *J. Appl. Phys.* **1997**, *81*, 6390−6396.

(4) Cartry, G.; Schiesko, L.; Hopf, C.; Ahmad, A.; Carrère, M.; Layet, J. M.; Kumar, P.; Engeln, R. Production of negative ions on graphite surface in H_2/D_2 plasmas: Experiments and SRIM calculations. *Phys. Plasmas* **2012**, *19*, No. 063503.

(5) Cacciatore, M.; Rutigliano, M. Recombination processes involving H and D atoms interacting with a graphite surface: collisional data relevant to fusion plasma devices. *Phys. Scr.* **2006**, *T124*, 80−85.

(6) Yamashina, T.; Hino, T. Plasma-surface interactions of graphite as nuclear fusion material. *Appl. Surf. Sci.* **1991**, *48−49*, 483−497.

(7) Qazi, M.; Vogt, T.; Koley, G. Trace gas detection using nanostructured graphite layers. *Appl. Phys. Lett.* **2007**, *91*, No. 233101.
(8) Shao, Y.; Wang, J.; Wu, H.; Liu, J.; Aksay, I. A.; Lin, Y. Graphene Based Electrochemical Sensors and Biosensors: A Review. *Electroanalysis* **2010**, *22*, 1027−1036.
(9) Rutigliano, M.; Pirani, F. Selectivity in the inelastic rotational scattering of hydrogen molecules. *Chem. Phys.* **2016**, *479*, 11−19.
(10) Rutigliano, M.; Pirani, F. On the influence of rotational motion of oxygen molecules on the scattering from graphite surfaces. *J. Phys. Chem. C* **2019**, *123*, 11752−11762.
(11) Rutigliano, M.; Pirani, F. Selectivity and Stereodynamics Effects in the Scattering of Nitrogen Molecules from a Graphite Surface. *J. Phys. Chem. C* **2020**, *124*, 10470−10482.
(12) Rutigliano, M.; Pirani, F. Selectivity in the inelastic rotational scattering of D_2 and HD molecules from graphite: Similarities and differences respect to the H_2 case. *Chem. Phys.* **2018**, *504*, 38−47.
(13) Pirani, F.; Brizi, S.; Roncaratti, L. F.; Casavecchia, P.; Cappelletti, D.; Vecchiocattivi, F. Beyond the Lennard-Jones model: a simple and accurate potential function probed by high resolution scattering data useful for molecular dynamics simulations. *Phys. Chem. Chem. Phys.* **2008**, *10*, 5489−5503.
(14) Billing, G. D. *Dynamics of Molecule Surface Interactions*; JohnWiley & Sons: New-York, 2000.
(15) Aquilanti, V.; Ascenzi, D.; de Castro Vitores, M.; Pirani, F.; Cappelletti, D. A quantum mechanical view of molecular alignment and cooling in seeded supersonic expansions. *J. Chem. Phys.* **1999**, *111*, 2620−2632.
(16) Aquilanti, V.; Ascenzi, D.; Cappelletti, D.; Fedeli, R.; Pirani, F. Molecular beam scattering of nitrogen molecules in supersonic seeded beams: a probe of rotational alignment. *J. Phys. Chem. A* **1997**, *101*, 7648−7656.
(17) Rivero Santamaría, A. R.; Alducin, M.; Díez Muiño, R.; Juaristi, J. I. Ab Initio Molecular Dynamics Study of Alignment-Resolved O_2 Scattering from Highly Oriented Pyrolytic Graphite. *J. Phys. Chem. C* **2019**, *123*, 31094−31102.
(18) Majumder, M.; Gibson, K. D.; Sibener, S. J.; Hase, W. L. Chemical Dynamics Simulations and Scattering Experiments for O_2. *J. Phys. Chem. C* **2018**, *122*, 16048−16059.
(19) Mehta, N. A.; Murray, V. J.; Xu, C.; Levin, D. A.; Minton, T. K. Nonreactive Scattering of N_2 from Layered Graphene Using Molecular Beam Experiments and Molecular Dynamics. *J. Phys. Chem. C* **2018**, *122*, 9859−9874.
(20) Majumder, M.; Bhandari, B. N.; Pratihar, S.; Hase, W. L. Chemical Dynamics Simulation of Low Energy N_2 Collisions with Graphite. *J. Phys. Chem. C* **2018**, *122*, 612−623.
(21) Oh, J.; Kondo, T.; Arakawa, K.; Saito, Y.; Nakamura, J.; Hayes, W. W.; Manson, J. R. Scattering of CO and N_2 molecules by a graphite surface. *J. Phys.: Condens. Matter* **2012**, *24*, No. 354001.
(22) Marchon, B.; Tysoe, W. T.; Carrazza, J.; Heinemann, H.; Somorjai, G. A. Reactive and Kinetic Properties of Carbon Monoxide and Carbon Dioxide on a Graphite Surface. *J. Phys. Chem. A* **1988**, *92*, 5744−5749.
(23) Beitel, G. A. Adsorption of Carbon Monoxide and Hydrogen on graphite. *J. Vac. Sci. Technol.* **1972**, *9*, 370−372.
(24) Patel, D. M.; Kodgire, P.; Dwived, A. H. Low temperature oxidation of carbon monoxide for heat recuperation: A green approach for energy production and a catalytic review. *J. Cleaner Prod.* **2020**, *245*, No. 118838.
(25) Gerbi, A.; Savio, L.; Vattuone, L.; Pirani, F.; Cappelletti, D.; Rocca, M. Role of Rotational Alignment in Dissociative Chemisorption and Oxidation: O_2 on Bare and CO-Precovered Pd(100). *Angew. Chem., Int. Ed.* **2006**, *45*, 6655−6658.
(26) Vattuone, L.; Gerbi, A.; Cappelletti, D.; Pirani, F.; Gunnella, R.; Savio, L.; Rocca, M. Selective Production of Reactive and Nonreactive Oxygen Atoms on Pd(001) by Rotationally Aligned Oxygen Molecules. *Angew. Chem., Int. Ed.* **2009**, *48*, 4845−4848.
(27) Lončarić, I.; Füchsel, G.; Juaristi, J. I.; Saalfrank, P. Strong Anisotropic Interaction Controls Unusual Sticking and Scattering of CO at Ru(0001). *Phys. Rev. Lett.* **2017**, *119*, No. 146101.
(28) Rutigliano, M.; Zazza, C.; Sanna, N.; Pieretti, A.; Mancini, G.; Barone, V.; Cacciatore, M. Oxygen Adsorption on β-Cristobalite Polymorph: Ab Initio Modeling and Semiclassical Time-Dependent Dynamics. *J. Phys. Chem. A* **2009**, *113*, 15366−15375.
(29) Rutigliano, M.; Gamallo, P.; Sayós, R.; Orlandini, S.; Cacciatore, M. A molecular dynamics simulation of hydrogen atoms collisions on an H-preadsorbed silica surface. *Plasma Sources Sci. Technol.* **2014**, *23*, No. 045016.
(30) Rutigliano, M.; Cacciatore, M. Eley−Rideal recombination of hydrogen atoms on a tungsten surface. *Phys. Chem. Chem. Phys.* **2011**, *13*, 7475−7484.
(31) Huber, K. P.; Herzberg, G. *Molecular Spectra and Molecular Structure: IV. Constants of Diatomic Molecules*; Van Nostrand Reinhold company: New York, 1979.
(32) Muckerman, J. T. Monte Carlo Calculations of Energy Partitioning and Isotope Effects in Reactions of Fluorine Atoms with H_2, HD, and D_2. *J. Chem. Phys.* **1971**, *54*, 1155−1164.
(33) Wyckoff, R. W. G. *Crystal Structures*; Wiley: New York, 1964.
(34) Sahni, R. C.; La Budde, C. D.; Sawhney, B. C. Quantum mechanical treatment of molecules. Part 1.Calculation of the potential energy curve and molecular constants of the ground state of CO. *Trans. Faraday Soc.* **1966**, *62*, 1993−2003.
(35) Rubeš, M.; Kysilka, J.; Nachtigallb, P.; Bludsky, O. DFT/CC investigation of physical adsorption on a graphite (0001) surface. *Phys. Chem. Chem. Phys.* **2010**, *12*, 6438−6444.
(36) Zhang, Y.-H.; Chen, Y.-B.; Zhou, K.-G.; Liu, C.-H.; Zeng, J.; Zhang, H.-L.; Peng, Y. Improving gas sensing properties of graphene by introducing dopants and defects: a first-principles study. *Nanotechnology* **2009**, *20*, No. 185504.
(37) Hosseinnejad, T.; Abdullah Mirzaei, R.; Nazari, F.; Karimi-Jafari, M. H. Adsorption behavior of CO and C_2H_2 on the graphite basal surface: a quantum chemistry study. *J. Struct. Chem.* **2013**, *54*, 850−856.
(38) Vidali, G.; Ihm, G.; Kim, H.-Y.; Cole, M. W. Potentials of physical adsorption. *Surf. Sci. Rep.* **1991**, *12*, 133−181.
(39) Piper, J.; Morrison, J. A.; Peters, C. The adsorption of carbon monoxide on graphite. *Mol. Phys.* **1984**, *53*, 1463−1480.
(40) Cambi, R.; Cappelletti, D.; Liuti, G.; Pirani, F. Generalized correlations in terms of polarizability for van der Waals interaction potential parameter calculations. *J. Chem. Phys.* **1991**, *95*, 1852−1861.
(41) Pirani, F.; Maciel, G. S.; Cappelletti, D.; Aquilanti, V. Experimental benchmarks and phenomenology of interatomic forces: open-shell and electronic anisotropy effects. *Int. Rev. Phys. Chem.* **2006**, *25*, 165−199.
(42) Israelachvili, J. N. *Intermolecular and Surface Forces*; Academic Press: London, 2011.
(43) Incze, A.; Pasturel, A.; Chatillon, C. Oxidation of graphite by atomic oxygen: a first-principles approach. *Surf. Sci.* **2003**, *537*, 55−63.

https://doi.org/10.1021/acs.jpcc.1c00555
J. Phys. Chem. C 2021, 125, 9074−9084